INEEL/CON-99-00472
PREPRINT

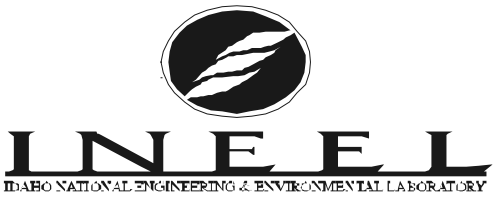

Dynamic Holographic Lock-In Imaging of Ultrasonic Waves

K. L. Telschow
V. A. Deason
S. K. Datta

17th Symposium on Energy Engineering Science

LOCKHEED MARTIN

DYNAMIC HOLOGRAPHIC LOCK-IN IMAGING OF ULTRASONIC WAVES

K. L. Telschow, V. A. Deason

Idaho National Engineering and Environmental Laboratory
Lockheed Martin Idaho Technologies Co.
Idaho Falls, ID 83415-2209

S. K. Datta

Department of Mechanical Engineering
University of Colorado
Boulder, CO 80309-0427

ABSTRACT

A laser imaging approach is presented that utilizes the adaptive property of photorefractive materials to produce a real-time measurement of ultrasonic traveling wave surface displacement and phase in all planar directions simultaneously without scanning. The imaging method performs optical lock-in operation. A single antisymmetric Lamb wave mode image produces direct quantitative determination of the phase velocity in all planar directions showing plate stiffness anisotropy. Excellent agreement was obtained with modeling calculations of the phase velocity in all planar directions for an anisotropic sheet material. The approach functions with diffusely scattering surfaces, subnanometer motions and at frequencies from Hz to GHz.

INTRODUCTION

A powerful method for imaging ultrasonic motion has been developed at the INEEL that utilizes the photorefractive effect in optically nonlinear materials to perform adaptive interferometry.[1,2] Optical interference is developed within a photorefractive material with this technique and the output is an optical image whose intensity distribution is directly proportional to the surface vibration amplitude, for small ultrasonic displacements. Utilizing this approach, no postprocessing of the data recorded by a video camera is required to produce images of the surface vibration amplitude over large areas. Application of this approach, referred to as the *INEEL Laser Ultrasonic Camera*, to imaging of standing wave resonant motion in plates has been previously described.[3,4,5] This paper describes optical lock-in operation of this imaging method by recording the nonstationary waveform of a traveling Lamb wave in a plate.[6]

PHOTOREFRACTIVITY BACKGROUND

Photorefractivity refers to that process where optical excitation and transport of charge carriers within select nonlinear optical materials produces a diffraction grating or hologram from the interference pattern developed inside the material. A spatial and temporal charge distribution results in the photorefractive material that reflects the phase information impressed onto an optical signal beam (e.g. by a vibrating surface). The INEEL method records the photorefractive grating produced at a fixed beat frequency between the phase modulated signal and reference beams. It can directly measure vibration amplitude and phase with a response proportional to the Bessel function of order one, providing a linear output for small amplitudes. The method accommodates rough surfaces, exhibits a flat frequency response above the photorefractive response cutoff frequency, and can be used for detecting both standing and traveling waves.

EXPERIMENTAL METHOD

The experimental setup for vibration detection is shown in Figure 1. A solid state laser source at 532 nm was split into two legs forming the signal and reference beams. The signal beam was reflected off traveling waves produced at the surface of a plate driven at its center by a continuously excited piezoelectric transducer. The traveling wave motion occurring on the plate surface produced a phase modulation δ_{sig} of the signal beam. The reference beam was phase modulated by an electro-optic modulator at a fixed modulation depth δ_{ref}. The modulated beams were combined and interfered inside a Bismuth Silicon Oxide (BSO) photorefractive crystal with operation in the diffusive regime. In the four-wave mixing configuration, the reference beam was reflected back into the crystal along a counter-propagating path that matched the Bragg angle of the photorefractive grating in the medium. The vibration modulated phase grating was read out by

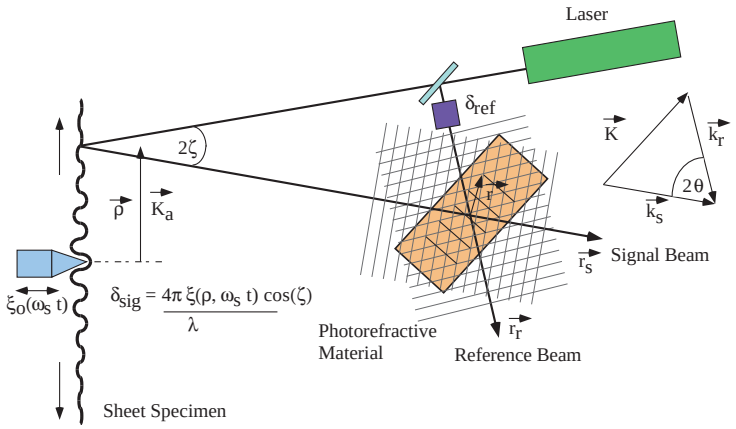

Figure 1. Optical Lock-in Ultrasonic Imaging Setup.

the resulting scattered wave that propagated backward along the signal beam leg and was detected by deflecting it with a beamsplitter (not shown) toward a photodetector or a video camera.

FLEXURAL WAVE DISPLACEMENT DISTRIBUTION

The lock-in mechanism that allows recording of ultrasonic wave displacements can be illustrated by considering a traveling flexural wave in a plate[7]. The displacement normal to the plate surface of a wave from an oscillating point excitation force F_0, for wavelengths larger than the plate thickness, is given by[8] $\xi(\rho,t) = \mathrm{Re}(i\xi_0\,[H_0^1(k_a\rho) - H_0^1(ik_a\rho)]e^{-i(\omega_s t+\varphi_s)})$ where $\xi_0 \equiv \dfrac{F_0}{8\omega\sqrt{D\sigma}}$, $k_a = \dfrac{2\pi}{\lambda_a}$ and $H_0^1(x)$ is the Hankel function of order zero representing a wave traveling outward from the origin. $D \equiv \dfrac{Eh^3}{12(1-s^2)}$ is the bending stiffness of the plate, $\sigma \equiv \rho_m h$ the mass density per unit area, ρ_m = the mass density, s = Poisson's ratio, E = Young's modulus and h = the plate thickness. The 2-dimensional spatial Fourier transform yields poles at the propagation wavevector $k_a^4 \equiv \dfrac{\sigma\omega^2}{D}$ as $\tilde{\xi}_\rho(q) = \dfrac{F_0}{D}\left[\dfrac{1}{(q^2-k_a^2)(q^2+k_a^2)}\right]$.

OPTICAL LOCK-IN TRAVELING WAVE DETECTION

The method by which the optical lock-in process demodulates the phase information can be illustrated by considering the four-wave mixing detection process. The Hankel function can be

written as $H_0^1(x) = h_0(x)\, e^{i(x-\frac{\pi}{4})}$ to configure the optical phase shift of the signal beam as $\Phi_{sig}(\rho,t) = \frac{4\pi\xi(\rho,t)}{\lambda} = \frac{4\pi}{\lambda}\xi_0 \left|h(k_a\rho)\right| \sin(\omega_s t + \varphi_s - k_a\rho + \frac{\pi}{4} - \Phi_a)$, where $\left|h(k_a\rho)\right| e^{i\Phi_a} \equiv h_0(k_a\rho) - h_0(ik_a\rho)e^{-k_a\rho(1+i)}$. Using the relation $e^{ix\sin(\theta)} = \sum_{n=-\infty}^{n=\infty} J_n(x)e^{in\theta}$ and $\Phi_{sig0} = \frac{4\pi\xi_0}{\lambda}$, the optical signal beam amplitude becomes

$$A_s(r,t) = A_{s0}\, e^{i(\vec{k}_s\cdot\vec{R}_s - 2\pi\nu t)} \sum_{n=-\infty}^{n=\infty} J_n(\delta_{sig0})\, e^{in(\omega_s t + \varphi_s - k_a\rho + \frac{\pi}{4} - \Phi_a)}$$

where $\vec{R}_s = \vec{r} + \vec{r}_s$, $\delta_{sig0} = \Phi_{sig0}\left|h(k_a\rho)\right|$ and ν is the laser optical frequency. The reference beam is similarly phase modulated by an electro-optic modulator (EOM) according to $\delta_{ref} = \delta_{ref0}\sin(\omega_r t + \varphi_r)$. $\delta_{sig0}, \delta_{ref0}$ are the magnitudes, ω_s, ω_r are the modulation frequencies and $\vec{r}_s, \vec{r}_r$ are the standoff distances and φ_s, φ_r are the modulation phases imposed by the specimen (signal) and the electro-optic modulator (reference), respectively.

Interference inside the crystal produces a spatially and temporally modulated intensity pattern with $\vec{K} = \vec{k}_s - \vec{k}_r$ the grating wavevector and $\Sigma = \vec{k}_s\cdot\vec{r}_s - \vec{k}_r\cdot\vec{r}_r$ accounting for path length differences between the two beams. The interference intensity distribution within the crystal generates a corresponding space charge electric field distribution. The dynamic behavior of this field is controlled by the charge carrier mobility and trapping that produces, in the diffusive operation regime, a single relaxation time response given by $\frac{\partial E_{sc}}{\partial t} + \frac{E_{sc}}{\tau} = \frac{iE_q}{\tau}\frac{2A_s\cdot A_r^*}{I_0}$, where τ, the material response time and E_q, are controlled by properties of the photorefractive material and the fringe spacing. In the above configuration, the photorefractive crystal acts as a mixing and low pass filtering element providing the benefits of lock-in detection. Therefore the space charge field responds to slowly varying phase modulations occurring within the material response time allowing only the terms around the difference frequency $\Omega\tau \le 1$ to be important, assuming $\Omega << \omega_{s,r}$. With $\Omega = \omega_r - \omega_s$, $\Phi = \varphi_r - \varphi_s$, $\tan(\psi_n) = n\Omega\tau$, and $\chi(\rho) = (k_a\rho - \frac{\pi}{4} + \Phi_a)$, the resultant space charge field becomes $E_{sc}(\vec{r},t) = E_q M\, f(\delta_{sig0}(\rho), \chi(\rho); t)\sin(\vec{K}\cdot\vec{r} + \Sigma)$, with

$$f(\delta_{sig0}(\rho), \chi(\rho); t) = \left[\begin{array}{l} J_0(\delta_{ref0})J_0(\delta_{sig0}(\rho)) + \\ 2J_1(\delta_{ref0})J_1(\delta_{sig0}(\rho))\frac{\cos(\Omega t + \Phi - \chi(\rho) - \psi_1)}{\sqrt{1+\Omega^2\tau^2}} + \ldots \end{array} \right]$$

where J_n is the Bessel function of the first kind.

The space-charge field modulates the local refractive index through the linear electro-optic effect. This effect creates a diffraction grating within the crystal that contains the low frequency phase information desired. The magnitude of the index of refraction grating produced is

$n_1 = \frac{n_0^3 r_{41} E_{sc}}{2}$, where n_0 is the average refractive index of the medium, r_{41} is the effective, orientation-dependent electro-optic coefficient. The diffraction efficiency of the grating is determined by the wave coupling constant $\zeta \equiv \left| \frac{\pi n_1 L}{\lambda \cos\theta} \right| = \frac{\Gamma L}{2} M\, f(\delta_{sig0}, \chi; t)$ where L is the interaction length, $\Gamma \equiv \frac{\pi n_0^3 r_{41} E_q}{\lambda \cos\theta}$ is the quadrature phase grating two-wave mixing coupling constant, λ is the source wavelength, and 2θ is the angle between the mixing waves.

In the four-wave mixing arrangement, the reference beam that passes through the crystal is reflected back into the crystal and diffracts from the photoinduced grating retracing the signal beam path. In the undepleted pump approximation, the diffracted (conjugate) beam intensity is given by $I_4 = I_3 e^{-\alpha L/\cos\theta} |\sin\zeta|^2$, where I_3 is the back-propagated reference beam intensity and α is the material absorption coefficient[9]. The refractive index modulation amplitude generated by the mixing process is generally small, so that $\zeta << 1, \quad and \quad \sin(\zeta) \approx \zeta$. The first time varying or AC term in the intensity of the diffracted beam is given by $I_4 \propto \left(\frac{\Gamma L}{2}\right)^2 M^2 \left[\frac{4 J_0(\delta_{ref\,0}) J_1(\delta_{ref\,0})}{\sqrt{1+\Omega^2\tau^2}}\right] J_0(\delta_{sig0}) J_1(\delta_{sig0}) \cos(\Omega t + \Phi - \chi(\rho) - \psi)$ where $\tan(\psi) = \Omega\tau$. This result shows that the magnitude and phase of the traveling wave have been placed into the arguments of the Bessel functions for the magnitude and as the phase of a low frequency AC signal. The resultant measured intensity, for small traveling wave displacement, is $I_{AC} \propto \frac{\delta_{sig0}}{2} \cos(\Omega t + \Phi - \chi(\rho) - \psi) \quad \propto \frac{4\pi\xi(\rho, \Omega t + \vartheta)}{\lambda}, \quad \vartheta = \Phi - \psi(\Omega\tau) + \frac{\pi}{2}$. The imaging approach provides a measure of both the traveling wave amplitude and phase for small amplitudes relative to the optical wavelength, ($\frac{4\pi\xi(\rho,t)}{\lambda} << 1$). The maximum detectable signal amplitude occurs at a phase shift of about one radian, corresponding to a traveling wave amplitude of about 45 nm for a probe wavelength of 532 nm.

OPTICAL LOCK-IN IMAGING

Since optical interference and the photorefractive effect occur throughout the photorefractive crystal, lock-in detection of the vibration over many points on the surface of the plate can be performed simultaneously. The volume character of the photorefractive process creates a grating distribution that locally records the phase modulation measured from each point of the specimen surface as long as the surface is accurately represented within the photorefractive crystal. The output beam intensity can then be measured by a CCD camera. Each pixel records the local intensity from a point on the specimen producing an output proportional to that point's

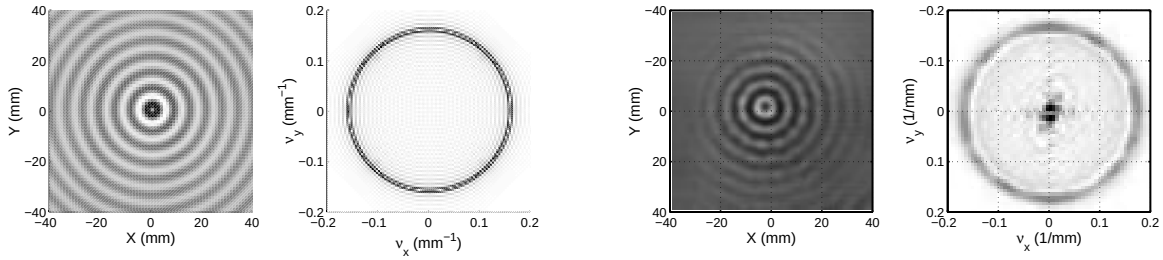

Figure 2: Calculated (left) and Measured (right) Traveling Wave Displacements and Magnitude of the 2-D FFT for the Nickel Plate at 30.0 kHz.

displacement. Even a diffusely reflecting surface can be measured if the surface is adequately imaged inside the photorefractive crystal by suitable optics.

Figure 2 shows an image of a traveling flexural wave in a 0.125 mm thick nickel plate at 30 kHz with $E = 204\ GPa$, $s = 0.31$, $\rho_m = 8.9\ g/cm^3$. The expected circular wavefronts due to the isotropic microstructure of the nickel plate are clearly defined and the ultrasonic displacement phase is readily distinguishable. The figure shows single frame image data. The entire pattern can be made to change its phase continuously at the frequency, Ω, from about 1–30 Hz, so that the appearance is that of waves emanating from the center and traveling outward. This is physically equivalent to the actual traveling wave motion except that viewing of the wave has been slowed to a much smaller observation frequency that is held constant and independent of the actual wave frequency. The photorefractive process yields a true picture of the actual wave vertical displacement motion and requires no additional processing for the images of Figure 2.

The magnitude of the Fourier transform of the traveling wave displacement shows real poles at the wavevector for the traveling wave and imaginary poles of the same magnitude that contribute to satisfy the boundary conditions. Therefore, the Fourier transform image of the traveling wave displacement image is a single ring at the wavevector delineating the propagating mode. Figure 2 shows images of the calculations and measurements of the traveling wave displacements. Also shown are images of the magnitudes of the Fourier transforms. A strong response is seen as a ring at the propagating wavevector that can be immediately measured to quantitatively show the elastic constants and the isotropic character of the plate. This analysis procedure provides considerable information about the plate in one simple image.

ANISOTROPIC MATERIAL MEASUREMENTS

If the specimen is elastically anisotropic, then the wave speed varies with the propagation direction. Figure 3 shows this type of behavior for traveling waves in a sheet of copy paper. The

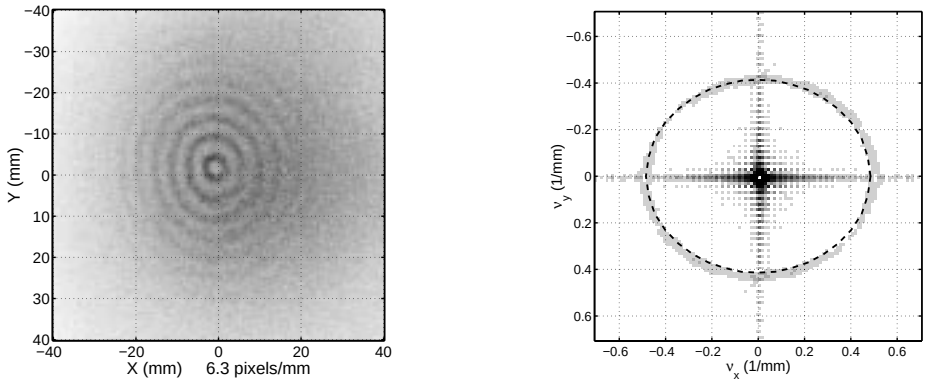

Figure 3: (left) INEEL Camera Image of Ultrasonic Waves In Paper, (right) Magnitude of the Fourier Transform of the Camera Image and Calculational Result (dashed lines).

paper sheet had its fibers aligned approximately along the vertical direction. The highly oblong wavefront pattern shows the anisotropy immediately. Modeling calculation of the elastic wave anisotropy for all planar angles has been performed from independent measurements of the elastic constant matrix for this paper material. Comparison with the image data provides direct measurement of the crystallographic axes orientation present in the material. Very good agreement between the calculations and the measurements can be seen at all directions in figure 3 and at all frequencies as shown in figure 4. Coupled with detailed modeling of this type, the *INEEL Laser Ultrasonic Camera* approach provides the an important step for developing a means of determining arbitrary orientations of anisotropic materials from wave images using data from all planar directions simultaneously.

CONCLUSIONS

An imaging optical lock-in traveling wave measurement method has been described. Direct two-dimensional surface images of the traveling wave were obtained by expanding the collection optics and imaging the output beam from the photorefractive material. These images showed the ultrasonic wavelength and wavefront shape in all planar directions and provided a quantitative method for obtaining the elastic stiffness of sheet materials, as illustrated for an isotropic nickel plate and an anisotropic sheet of paper. The method is capable of flat frequency response over a wide range above the reciprocal of the photorefractive time constant and is applicable to imaging the ultrasonic motion of surfaces with rough, diffusely reflecting finishes. Coupled with detailed modeling of anisotropic elastic properties of materials, imaging provides a powerful technique for microstructure measurement and analysis.

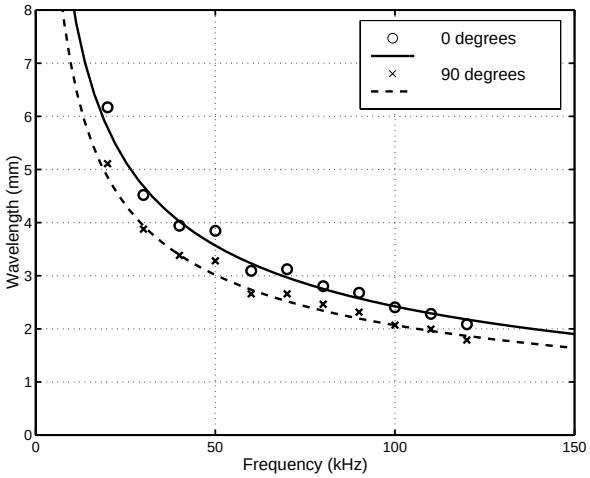

Figure 4. Measured and Calculated Wavelengths

ACKNOWLEDGMENTS

The authors thank S. M. Watson and R. S. Schley for experimental help, A. Jonas Niklasson for the modeling calculations, and Dr. J. Gerhartstein and Dr. P. Brodeur of the Institute of Paper Science and Technology, Atlanta, GA, for the elastic constant matrix for the paper sample. This work was sponsored by the U.S. Department of Energy, Office of Energy Research, Office of Basic Energy Sciences, Engineering Research and the INEEL Laboratory Directed Research & Development program under DOE Idaho Operations Office Contract DE-AC07-94ID13223.

REFERENCES

1 P. Yeh, *Introduction to Photorefractive Nonlinear Optics*, (John Wiley, New York, 1993).

2 S. I. Stepanov, *International Trends in Optics*, (Academic Press, New York, 1991) Ch. 9.

3 T. C. Chatters and K. L. Telschow, *Review of Progress in QNDE*, Vol. 15B, Eds. D.O. Thompson and D. E. Chimenti, (Plenum Press, New York, 1996) pp. 2,165–2,171.

4 T. C. Hale and K. Telschow, Appl. Phys. Lett. 69, 2,632–2,634 (1996).

5 T. C. Hale, K. L. Telschow, and V. A. Deason, Applied Optics, 111, 8,248–8,258 (1997).

6 K. L. Telschow, V. A. Deason, R. S. Schley and S. M. Watson, *Review of Progress in QNDE*, Vol. 18, Eds. D.O. Thompson and D. E. Chimenti, (Plenum Press, New York, 1999) to be published.

7 K.L. Telschow, V. A. Deason, R. S. Schley and S. M. Watson, "Direct Imaging of Lamb Waves in Plates using Photorefractive Dynamic Holography," to be published.

8 P. M. Morse and K. U. Ingard, *Theoretical Acoustics*, (McGraw-Hill, New York, 1968) 219.

9 H. Kogelnik, Bell System Technical Journal 48, 2,909–2,947 (1969).